Electronic states, bonding, and x-ray absorption spectra of Pd_2Si

O. Bisi
Physics Department, University of Modena, Via Campi 213/A, 41100 Modena, Italy

O. Jepsen and O. K. Andersen
Max-Planck-Institut fur Festkörperforschung, Heisenbergstrasse 1, 7000 Stuttgart 80, Federal Republic of Germany
(Received 4 May 1987)

The electronic properties of Pd_2Si are analyzed in light of a self-consistent calculation of the electronic states. By using the linear muffin-tin orbitals method in the atomic-sphere approximation, energy bands, densities of states, x-ray photoabsorption spectra, and the total energy have been determined. The basic bonding interaction between Pd and Si is found to be a bonding-antibonding coupling between Pd $4d$ and Si $3p$ orbitals. This leaves the Si $3s$ states in an atomic-like configuration. Many features of the experimental spectroscopic data can be interpreted using this overall picture, but there are details which depend on the complexities of the crystal structure. We found that the Si $3p$ states just below the Fermi level, often attributed to the filled portion of the Pd d–Si p antibonding states, are indeed due to a Pd p–Si p coupling. The antibonding states of this coupling are entirely unoccupied and are responsible for both the low-energy structure determined by bremsstrahlung isochromat spectroscopy (BIS) and the occurrence of the white line in the Pd $L_{2,3}$ x-ray absorption spectra. Furthermore, a Pd p–Si d structure provides an explanation of the higher-energy BIS features and of the main peak in the Pd L_1 absorption data. These results show that many-body effects are hardly necessary in order to interpret the existing x-ray absorption spectra. The zero-temperature heat of formation is calculated to be -11.3 kcal/g-at. and the room-temperature experimental value is -6.9 kcal/g-at.

I. INTRODUCTION

It is well known that the transition-metal–silicon contact reaction leads to the formation of silicide compounds.[1,2] Most of these compounds are metals, so what the reaction does is to replace the transition-metal–silicon interface with a rather stable silicide-silicon interface. The understanding of the chemical, structural, and electronic properties of these metal-silicon compounds has become an important issue from both scientific and technological points of view.[3–5]

The aim of the present work is to gain insight into the electronic and structural properties of the Pd-Si system through a detailed investigation of one of its stable compounds, Pd_2Si. For this purpose we performed a self-consistent density functional[6–10] calculation of the electronic states of Pd_2Si using the linear muffin-tin orbitals (LMTO) method in the atomic-sphere approximation (ASA).[11]

Palladium silicide Pd_2Si crystalizes in a rather complex structure with nonequivalent Pd and Si atoms and with a total of nine atoms per primitive cell. For this reason no first-principles calculation of its electronic properties had previously been performed. We analyzed the x-ray absorption spectra (XAS) through the evaluation of the one-electron photoabsorption spectra within the dipole approximation.

The Pd_2Si crystal structure is described in Sec. II. In Sec. III we will illustrate briefly some technical details of our LMTO-ASA calculation. The self-consistent energy bands and density of states will be discussed in Sec. IV, and the details of the photoabsorption spectra calculation and the results are discussed in Sec. V. In the following section the computed total energy, cohesive energy, and heat of formation will be presented. The discussion of our results and the comparison with experimental data, in particular spectroscopic experiments for both occupied and empty valence states, are the subjects of Sec. VII. Finally, the principal conclusions of this work are summarized in Sec. VIII.

II. CRYSTAL STRUCTURE

Pd_2Si forms a hexagonal system with three molecules per primitive cell.[12] The crystal structure data are listed in Table I. Figure 1 shows the atomic sites inside the hexagonal cell which is formed by two hexagonal planes at a distance of $c/2$. Due to the fact that the two basal planes display different atomic sites, we have two nonequivalent Si and Pd atoms inside the unit cell. We will label them by the index (1) and (2), respectively (see Fig. 1). We remark that the stoichiometry of the two basal planes is different, the first plane being Pd_3Si_2, the second Pd_3Si. The basal plane of Pd_2Si and the Si(111) surface present a lattice mismatch of only 2% which leads to epitaxial growth of Pd_2Si on Si(111).[13]

The interatomic distances shorter than 3.6 Å and their coordination number are listed in Table II. Both Si(1) and Si(2) atoms have three Pd atoms on the same plane at 2.45 or 2.63 Å and six Pd atoms at the vertices of a triangular prism with the basis on the adjacent planes (distance of 2.61 or 2.39 Å). Each Pd atom has 11 or 12

TABLE I. Structural data for Pd_2Si.

Crystallographic data	Lattice constants	Primitive cell volume
Hexagonal system	$a=6.49$ Å	$\Omega=125.12$ Å^3 (real space)
$C22$ structure type	$c=3.43$ Å	$\Omega_k=1.98$ Å^{-3} (reciprocal space)
$P\bar{6}2m$ space group	$c/a=0.528$	

neighbors within 2.88 Å, to be compared with the 12 first-neighbors shell at 2.75 Å found in elemental Pd with fcc structure. For both Pd(1) and Pd(2) atoms the first shells of Pd atoms lie between 2.78 and 2.88 Å, but in Pd(1) we have eight neighbors at this distance, while in Pd(2) only six Pd atoms are present. This fact will produce different features in the site-projected electronic density of states (DOS), as will be shown in Sec. IV.

III. DETAILS OF THE CALCULATION

A detailed description of the LMTO-ASA method, including its use for compounds, is given elsewhere.[14,15] The present calculations were carried out semirelativistically and retained components through $l=2$ in the angular momentum basis.

In the atomic spheres approximation the muffin-tin interstitial region is "annihilated" through the expansion of the muffin-tin spheres and the neglect of the slight overlap. The muffin-tin spheres in this approximation thus become the Wigner-Seitz spheres which are supposed to fill space. The potential is taken to be spherically symmetric within the spheres.

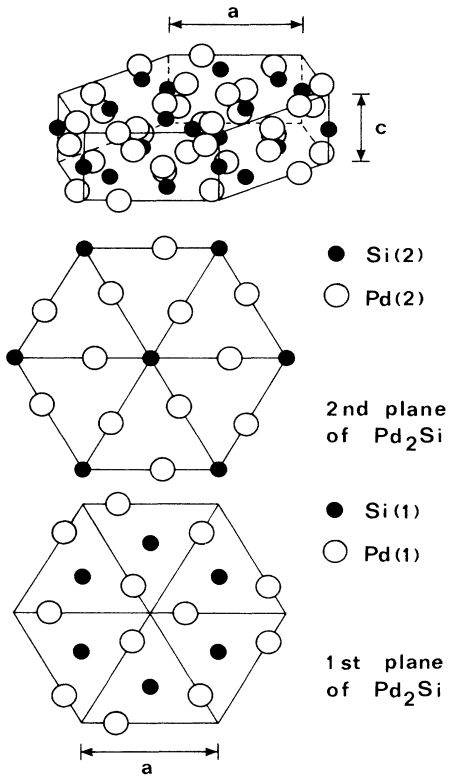

FIG. 1. The silicon and palladium atomic sites in the two alternating planes normal to the c axis and in the three-dimensional hexagonal cell in Pd_2Si. Both Si and Pd atoms are found in two nonequivalent sites, labeled by (1) and (2).

This approximation is valid for closely packed solids, i.e., when the touching spheres interstitial region $\Omega-\Omega^0$ is less than (of the order of) $\frac{1}{3}$ of the total volume Ω. In terms of the packing fraction $f=\Omega^0/\Omega$ we obtain $f=0.67$. By letting the nonequivalent Si and Pd atoms having slightly different muffin-tin spheres radii it is possible to reach a satisfactory packing of the solid ($f=0.66$). The Wigner-Seitz space-filling spheres radii S_t are shown in Table III. We observe that the ratio between the Pd and Si radii is close to the value 1.27 obtained by using atomic Slater orbitals.[16] The maximum overlap produced by the ASA approximation is $O_{i,j}(\max)=(f^{-1/3}-1)d_{i,j}=0.148d_{i,j}$, where $d_{i,j}$ is the i-j site distance.

The LMTO-ASA band-structure calculation presented here uses the "frozen-core" approximation, i.e., the inner-electron wave functions are taken from the self-consistent atomic calculations, and only the valence states are adjusted during the self-consistent cycles.

Exchange and correlation contributions to both atomic and crystalline potential have been included through the density-functional description in the local-density approximation (LDA).[6–8]

The k-integrated functions have been evaluated by the tetrahedron method[17] on a grid of 120 k points in the irreducible part of the Brillouin zone (BZ), of volume $\frac{1}{12}\Omega_k$.

Table III shows the input atomic Wigner-Seitz radii together with the LMTO output data, i.e., the potential parameters and the electronic configuration of Pd_2Si. The self-consistent energy bands and densities of states of Pd_2Si can be reconstructed by using the potential parameters of Table III, together with the structure con-

TABLE II. Interatomic distances (in Å) in Pd_2Si. Distances shorter than 3.6 Å are listed. The numbers in parentheses denotes the number of equivalent distances.

	Pd(1)	Pd(2)	Si(1)	Si(2)
Pd(1)	2.88 (2)	2.78 (2)	2.45 (2)	2.39 (2)
	3.43 (2)	2.88 (4)		
Pd(2)	2.78 (2)	3.41 (4)	2.61 (4)	2.63 (1)
	2.88 (4)	3.43 (2)		
Si(1)	2.45 (3)	2.61 (6)	3.43 (2)	
Si(2)	2.39 (6)	2.63 (3)		3.43 (2)

TABLE III. Atomic Wigner-Seitz radii, self-consistent potential parameters, as defined in Ref. 11, and the electronic configuration of Pd_2Si.

		Pd(1)	Pd(2)	Si(1)	Si(2)
S (Å)		1.50	1.60	1.39	1.24
E_v (Ry)	(s)	−0.5847	−0.5567	−0.7092	−0.7657
	(p)	−0.4137	−0.4245	−0.4223	−0.4377
	(d)	−0.3774	−0.3325	−0.3479	−0.3569
$\omega_v(-)$ (Ry)	(s)	0.1957	0.1675	−0.1438	−0.1944
	(p)	1.0397	0.9156	0.4701	0.5638
	(d)	0.0282	0.0169	1.7592	1.9773
$S\phi_v^2(-)$ (Ry)	(s)	0.3378	0.2819	0.2779	0.3999
	(p)	0.3276	0.2790	0.2393	0.3292
	(d)	0.0375	0.0284	0.2636	0.3210
$\phi_v(-)/\phi_v(+)$	(s)	0.8648	0.8593	0.8037	0.8194
	(p)	0.7100	0.7024	0.5848	0.5980
	(d)	0.0678	0.0485	0.5228	0.5084
$(\langle\dot{\phi}_v^2\rangle)^{-1/2}$ (Ry)	(s)	4.7556	3.8654	2.9866	4.3364
	(p)	6.4335	5.5227	3.9169	5.3966
	(d)	0.9823	0.7805	5.9037	7.0996
n (e/at.)	(s)	0.621	0.635	1.426	1.497
	(p)	0.892	0.896	2.044	2.049
	(d)	8.486	8.469	0.529	0.481

stants defined by Andersen.[11] It is interesting to analyze the differences between Pd(1) and Pd(2) and between Si(1) and Si(2). In spite of the different geometrical environment which causes some differences in the potential parameters, the electronic configuration of nonequivalent Pd and Si atoms is very similar. Therefore it is possible to introduce the Pd_2Si average electronic configuration which results to be $s^{0.6}p^{0.9}d^{8.5}$ for Pd and $s^{1.5}p^{2.0}d^{0.5}$ for Si.

IV. ENERGY BANDS AND DENSITY OF STATES

Figure 2 shows the Pd_2Si Brillouin zone, its irreducible part, and the main symmetry lines. Self-consistent valence bands for the directions $M'\Gamma$ and ΓA are plotted in Fig. 3. The Fermi level E_F is located at −0.106 Ry. Other symmetry directions, not shown, are characterized by similar features.

The characteristic features of the band structure may be described as follows: three low-lying bands centered

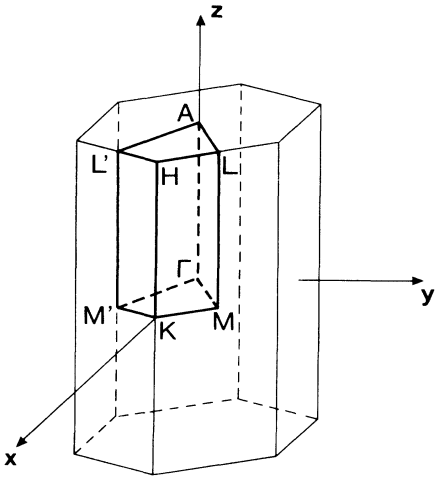

FIG. 2. The Brillouin zone of Pd_2Si and its irreducible part.

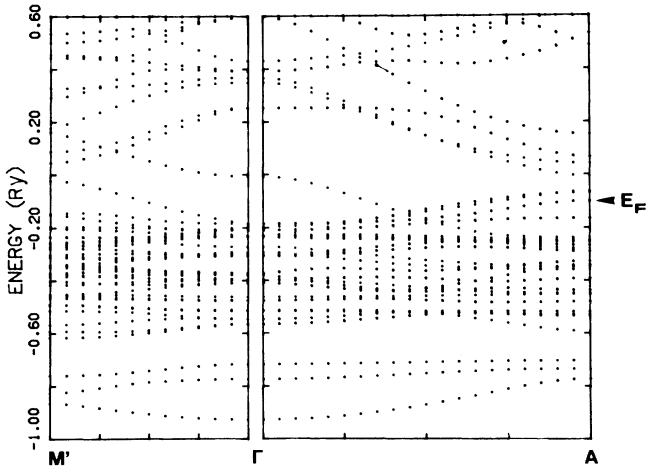

FIG. 3. Self-consistent energy band structure of Pd_2Si along the $M'\Gamma$ and ΓA directions. The Fermi level is located at −0.106 Ry.

around −0.8 Ry and of mainly Si s character are separated by a 90 mRy gap around −0.66 Ry from the rest of the bands. The remaining part of the filled bands are characterized by a very high density of states and with a width of about 0.4 Ry. These flat bands have mainly Pd d character and their high density is due to the large number of palladium atoms per unit cell.

Above E_F the electronic bands look differently. They are more dispersive with free-electron-like character. Above + 0.4 Ry, where the presence of Si d states is expected, the dispersion of the bands is reduced. It is important to notice that Pd d-derived states are found above E_F, for example near the A point. Furthermore, various hybridization features between d states and higher-energy, free-electron-like orbitals are present in this energy range. This hybridization produces an increase of the number of unoccupied d states, on passing from elemental Pd to Pd_2Si. The d-states configuration in Pd_2Si is indeed 8.478 electrons per atom, to be compared with the value of 8.601 found in elemental Pd.[14] Since the silicon present in Pd_2Si is expected to decrease the d-d interaction responsible for the d bandwidth of elemental Pd, towards a noble-metal-like configuration, a different mechanism should be responsible for the resultant d band widening and d occupancy decreasing. As we shall see, this new interaction, characteristic of the silicide, is due to the Si $3p$–Pd $4d$ coupling.

The total density of states and the total number of states (NOS) of Pd_2Si, obtained through the self-consistent LMTO-ASA calculation, are displayed in Fig. 4. These total spectra contain the contribution from the nine atoms of the unit cell, i.e., from 3 Pd(1), 3 Pd(2), 2 Si(1), and 1 Si(2) atoms. The partial DOS, in units of the number of states/(spin atom Ry) and the partial NOS in units of number of states/(spin atom) are displayed in Figs. 5–8 for the Pd(1), Pd(2), Si(1), and Si(2) atoms, respectively. From the analysis of these partial DOS curves the main features of the DOS curve can be interpreted and the basic interactions in Pd_2Si can be understood.

It is evident that the higher binding energy structure, separated by a gap from the rest of the valence band, is mainly due to the Si $3s$ states, weakly interacting with Pd s and p states. From the partial NOS curves of Figs. 5–8 it may be seen that every Si atom contributes about 0.5 s states/spin while the Pd s (p) contribution is limited to about 0.2 (0.1) states/spin. Unlike elemental Si the Pd_2Si $3s$ Si states are found in a "quasicore" configuration, without hybridizing with the $3p$ orbitals and only weakly

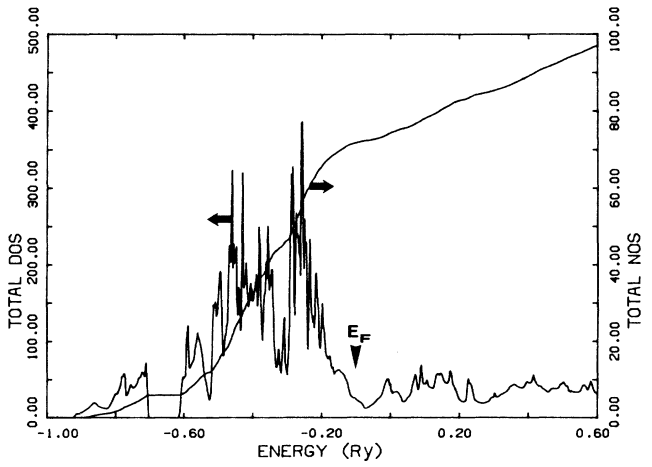

FIG. 4. Self-consistent total density of states (left axis) and total number of states (right axis) of Pd_2Si. Units are number of states/(cell Ry) (DOS) and number of states/cell (NOS). The Fermi level is located at −0.106 Ry.

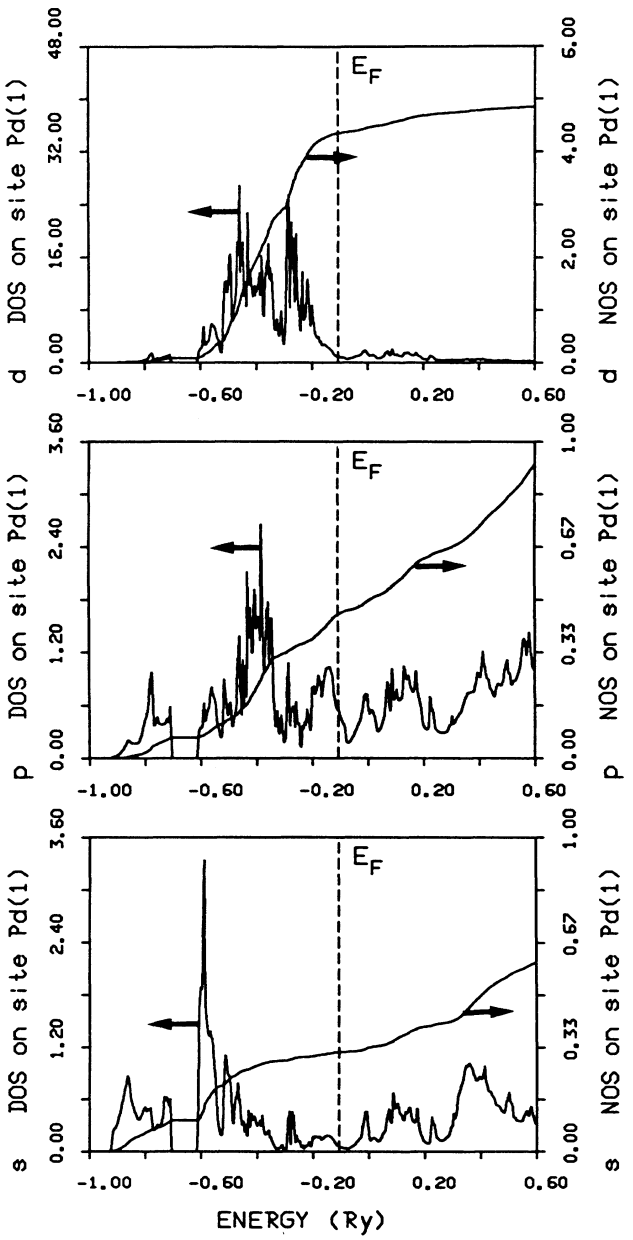

FIG. 5. Self-consistent Pd(1) s, p, and d partial densities of states (left axis) and partial number of states (right axis) of Pd_2Si. Units are number of states/(spin atom Ry) (DOS) and number of states/(spin atom) (NOS). The Fermi level is located at −0.106 Ry.

interacting with the Pd s and p states.

The remaining region of the occupied spectra, ranging from -0.62 Ry to E_F is dominated by the strongly structured Pd $4d$ states. In particular around -0.58 and -0.40 Ry we have the Pd s-d and p-d hybridization peaks; between them the DOS is dominated by the Si $3p$–Pd $4d$ interaction. The higher energy part of the DOS is characterized by a different interaction, mainly d-d, nonbonding coupling.

The Fermi level lies in a low-density region, the Pd_2Si DOS having the value of 22.8 states/(cell Ry) at this energy. The empty state region shows two different structures, centered around $+0.11$ and $+0.44$ Ry. The lower-energy peak is mainly due to the Si $3p$ states, interacting with Pd $4d$ orbitals. It constitutes the high-energy counterpart of the Si p–Pd d bonding coupling we found between -0.62 and -0.34 Ry. It means that the bonding interaction between Pd and Si may be merely described in terms of a two-level interaction between Pd $4d$ and Si $3p$ orbitals, forming bonding-antibonding

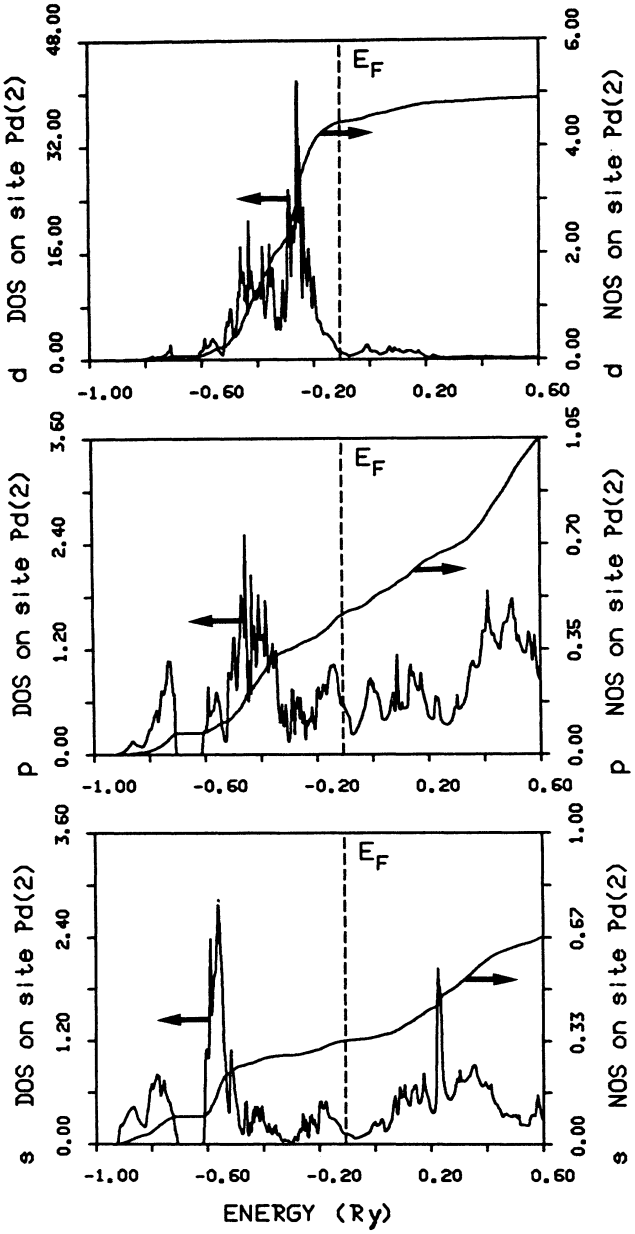

FIG. 6. Self-consistent Pd(2) s, p, and d partial densities of states (left axis) and partial number of states (right axis) of Pd_2Si. Units are number of states/(spin atom Ry) (DOS) and number of states/(spin atom) (NOS). The Fermi level is located at -0.106 Ry.

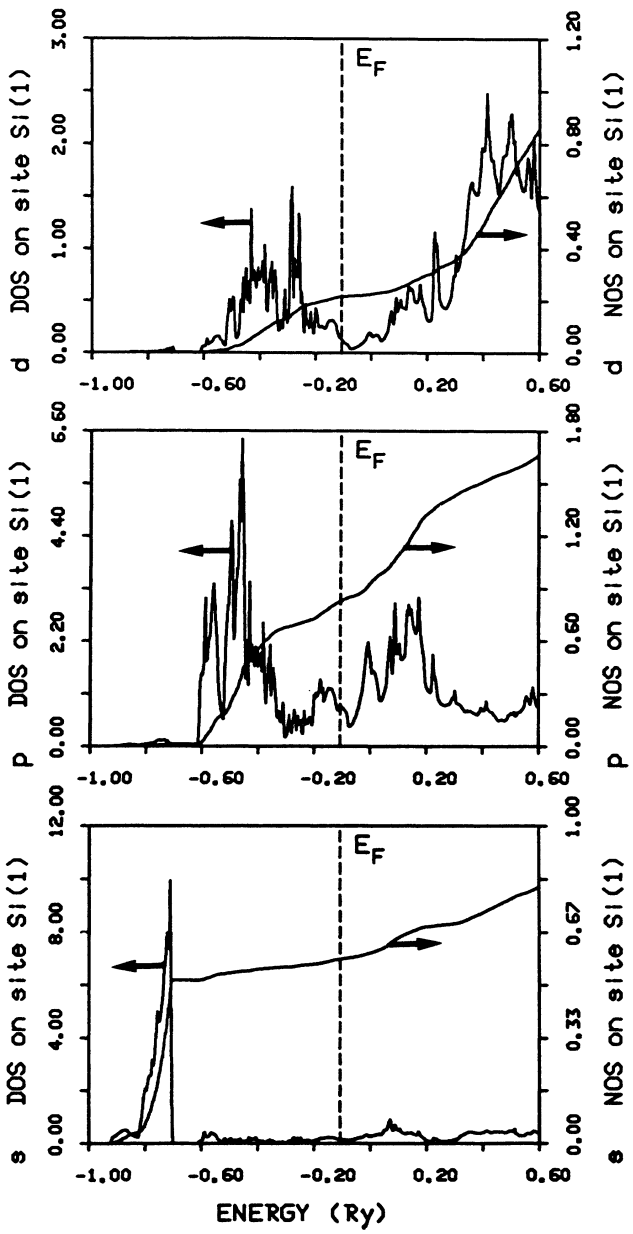

FIG. 7. Self-consistent Si(1) s, p, and d partial densities of states (left axis) and partial number of states (right axis) of Pd_2Si. Units are number of states/(spin atom Ry) (DOS) and number of states/(spin atom) (NOS). The Fermi level is located at -0.106 Ry.

states on both sites of the main nonbonding d structure. This result is in agreement with both augmented-spherical-wave (ASW) calculation of model PdSi and Pd_3Si compound[18] and with a tight-binding analysis of Pd_2Si.[19]

The higher-energy structure is due to a different kind of interaction between Pd and Si, i.e., a Pd $5p$–Si $3d$ coupling. At energies greater than $+0.3$ Ry above E_F the picture of the electronic states is more complex than the simple two-level description, new orbitals being involved in the basic interaction.

It should be stressed that the two-level coupling is only a simplified description of the interaction of a very complex Si-Pd system. It accounts for the qualitative picture of the Pd_2Si DOS, but various structures appear in our full calculation which are not explained in such simple terms. Relevant for the comparison with spectroscopic data is the Si p feature just below E_F (at -0.15 Ry). It has often been interpreted in terms of the filled portion of the antibonding Si p–Pd d states. On the contrary, as will be shown in Sec. VII, it can clearly be seen that this Si p feature does not show any coupling with the Pd d states which have negligible weight in this energy range. This interaction is therefore due to a different coupling, not described by the bonding-antibonding picture, namely a Si p–Pd p interaction.

The partial DOS of Figs. 5–8 show the similarity between the two inequivalent Pd atoms and the two inequivalent Si atoms. Only few differences exist; for example, the nonbonding d states below E_F are more peaked in Pd(2) than in Pd(1). The reason for this is the greater coordination number of the first shells of Pd atoms around Pd(1) than in Pd(2) (see Table II).

V. PHOTOABSORPTION SPECTRA

In x-ray absorption spectroscopy a core electron is excited to an empty state. This process will change the intensity I of the x-ray beam passing through a solid of thickness x according to the law $I=I_0e^{-\mu x}$, where μ is the absorption coefficient. In a single-particle picture the absorption coefficient due to the transitions from the core level with quantum number c and energy E_c is given by[20–22]

$$\mu_c(E)=\frac{4\pi^2}{3}\frac{\alpha\hbar\omega}{\Omega}\sum_{k,j}^{\text{unoccup}}|\langle c\,|\,\mathbf{r}\,|\,k,j\rangle|^2\delta(E(k,j)-E_c-\hbar\omega)\ , \tag{1}$$

where α is the fine-structure constant, Ω the cell volume, $\hbar\omega$ the photon energy, and k,j labels the single-particle unoccupied states.

Due to the spherical symmetry of the LMTO-ASA potential the dipole matrix elements of Eq. (1) lead to atomic selection rules which select the final-state symmetry according to the core state angular momentum l. We introduce the raw spectra $\hat{\mu}_c$ which is the probability of a photoabsorption transition from the core level to any valence state (filled or empty):

$$\hat{\mu}_c(E)=P_{l-1}N_{l-1}|\langle c,l\,|\,\mathbf{r}\,|\,k,j,l-1\rangle|^2+P_{l+1}N_{l+1}|\langle c,l\,|\,\mathbf{r}\,|\,k,j,l+1\rangle|^2\ . \tag{2}$$

Due to the strong localization of the core wave function the angular brackets in Eq. (2) select only the contribution of the atom in which the core-hole is created. The number of these atoms per cell, n_t, is included in the factor P_l which accounts for the empty-state spin degeneracy (2) and the core-level degeneracy d_c,

$$P_l=2\frac{4\pi^2}{3}\frac{\alpha\hbar\omega}{\Omega}\frac{d_c}{2l+1}n_t\ . \tag{3}$$

The function N_l is the l-projected density of states plotted in Figs. 5–8. Since we are concerned with the process of creating a core hole in a Pd atom in Pd_2Si, only the data of Figs. 5 and 6 will be used.

According to Eq. (2) two angular momenta contribute to the absorption coefficient, both of these being a product of the projected DOS and the matrix element term. These factors for $l-1$ and $l+1$ are displayed in Figs. 9 and 10, respectively. The computed spectra refer to the calculation of the Pd L_3 absorption spectra in the Pd_2Si environment, i.e., when the core hole is created in a $2p_{3/2}$ Pd state. Therefore Fig. 9 shows the s contribution to μ_c, while Fig. 10 shows the d contribution.

By comparing the s contribution of Fig. 9 with the d contribution of Fig. 10 we may see that the L_3 absorption spectra is dominated by the d states character, which is greater than the s part by a factor of 8 for the DOS and 70 for the matrix element. Furthermore, the computed matrix elements increase with the energy of the valence states, enhancing the relative weight of the high-energy states. By adding the s and d contributions we obtain the total raw spectra of Fig. 11. The similarity with the d-projected spectra is evident, the main difference being the matrix element enhancement of the higher-energy states, particularly the antibonding structure centered around 0.21 Ry above E_F.

The absorption coefficient μ_c is obtained from the raw spectrum $\hat{\mu}_c$ by introducing the valence state occupancy and the lifetime Lorentzian broadening:

$$\mu_c(E)=\frac{1}{2\pi}\int_{E_F}^{\infty}\frac{\hat{\mu}_c(E')\Gamma(E')}{(E'-E)^2+[\Gamma(E')/2]^2}dE'\ . \tag{4}$$

The broadening function is given by $\Gamma(E)=\Gamma_c+\Gamma_x(E)$, where Γ_c is the core-hole width and $\Gamma_x(E)$ is the width of the excited band energy. These broadening functions are not known for the Pd_2Si case. Data from elemental metals[21] show that in the energy range under study, i.e., for energies just above the edge threshold E_F, the core-

hole width is dominant. Therefore we approximate the broadening function $\Gamma(E)$ with the energy-independent core-hole width Γ_c. Due to the intra-atomic nature of the core-hole broadening, which is not very sensitive to the features of the chemical bond, the Γ_c of Pd_2Si is not expected to differ significantly from the elemental Pd value. Therefore the following core-hole width, found in elemental Pd (Refs. 21, 23, and 24) have been used also in the Pd_2Si calculation: $\Gamma_K=0.456$ Ry, $\Gamma_{L_1}=0.478$ Ry, $\Gamma_{L_3}=0.154$ Ry, and $\Gamma_{L_2}=0.184$ Ry. Note that we have not included any broadening due to the experimental resolution.

The computed absorption coefficient of the Pd_2Si Pd L_3 edge is shown in Fig. 11. The main peak at 0.2 Ry with intensity 0.315×10^{-4} a.u. (6000 cm^{-1}) is due to the presence of antibonding states and the enhancement effect of the matrix element. The shoulder at 0.5 Ry is due to the peak in the Pd $5s$-projected DOS (see Fig. 9).

We have performed a similar analysis for the Pd_2Si Pd K, L_1, and L_2 edges. The result for L_2 is very similar to the one shown for L_3. It is interesting to note that the intensity ratio $I(L_3)/I(L_2)$ turns out to be 2.2, very close to the core-level degeneracy ratio (2).

The total raw spectrum $\hat{\mu}_c$ and the absorption coefficient μ_c for the K edge are displayed in Fig. 12. In this case the $1s$ electron is excited and the absorption coefficient depends only on the $(l+1)5p$ valence contribution. Therefore the Pd d–Si p antibonding interaction produces only a weak shoulder, while the main $5p$ peak is found at 0.52 Ry. The results in Figs. 9–12 refer to a Pd(1) type atom. We found the corresponding Pd(2) results very similar, and the broadened μ_c spectra were indistinguishable.

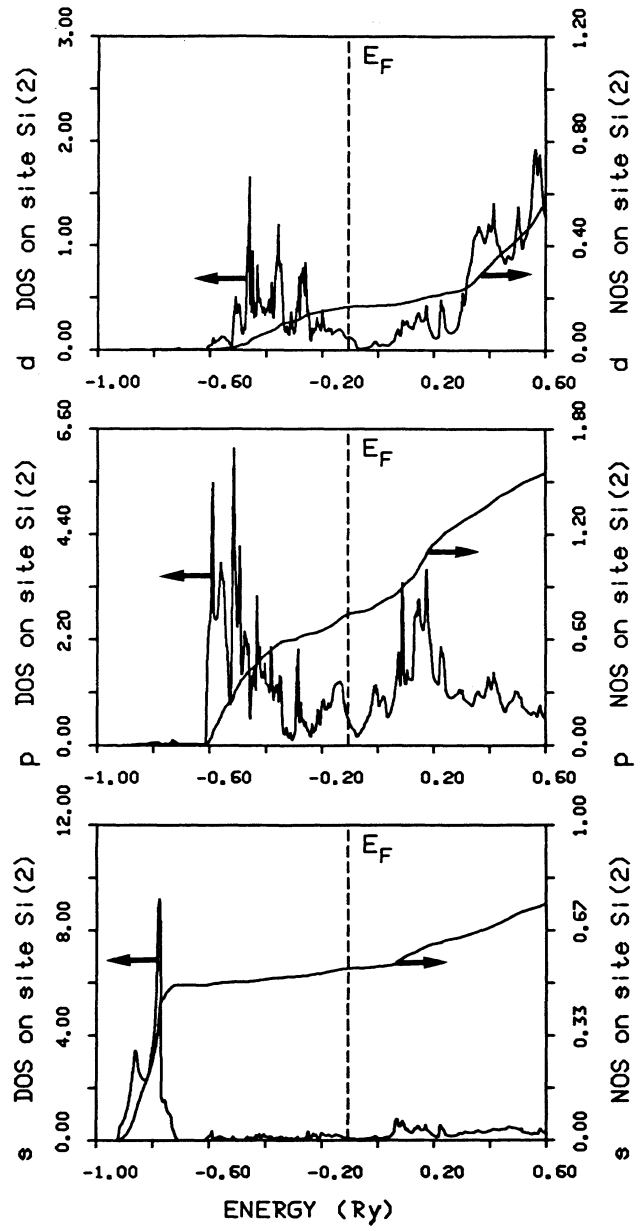

FIG. 8. Self-consistent Si(2) s, p, and d partial densities of states (left axis) and partial number of states (right axis) of Pd_2Si. Units are number of states/(spin atom Ry) (DOS) and number of states/(spin atom) (NOS). The Fermi level is located at −0.106 Ry.

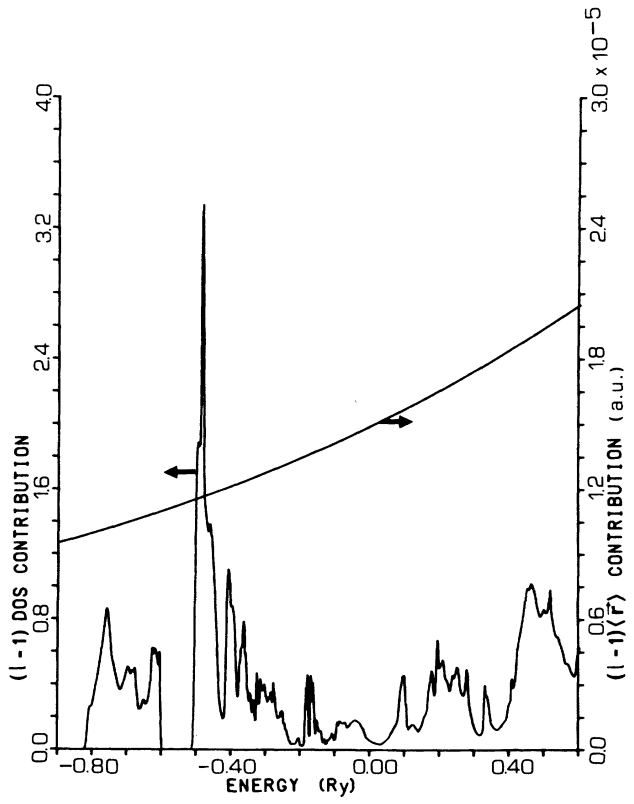

FIG. 9. Density of states (left axis) and matrix element (right axis) contributions to the raw absorption coefficient spectra of Pd_2Si. The calculation refers to the Pd L_3 edge and the $l-1(s)$ contributions are plotted. The Fermi level is located at zero energy and the left axis units are number of states/(spin atom Ry).

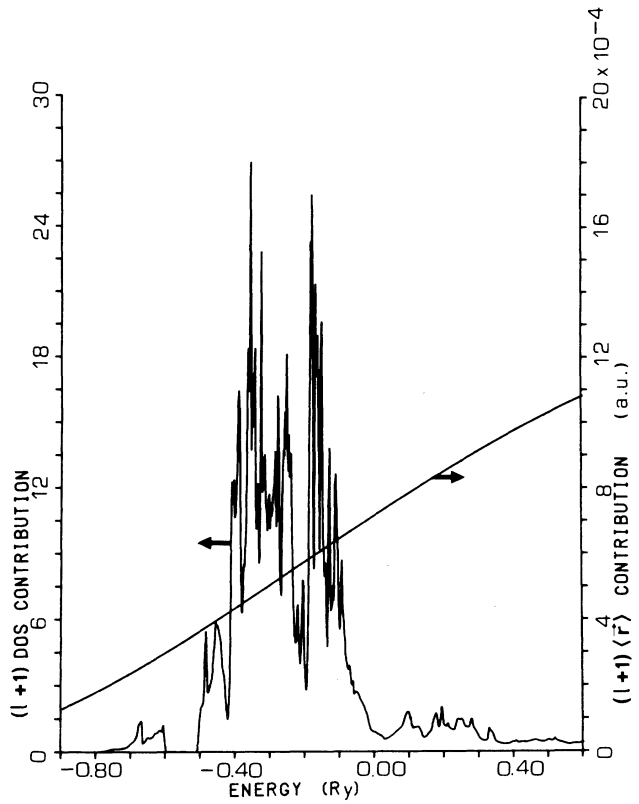

FIG. 10. Density of states (left axis) and matrix element (right axis) contributions to the raw absorption coefficient spectra of Pd_2Si. The calculation refers to the Pd L_3 edge and the $l+1(d)$ contributions are plotted. The Fermi level is located at zero energy and the left axis units are number of states/(spin atom Ry).

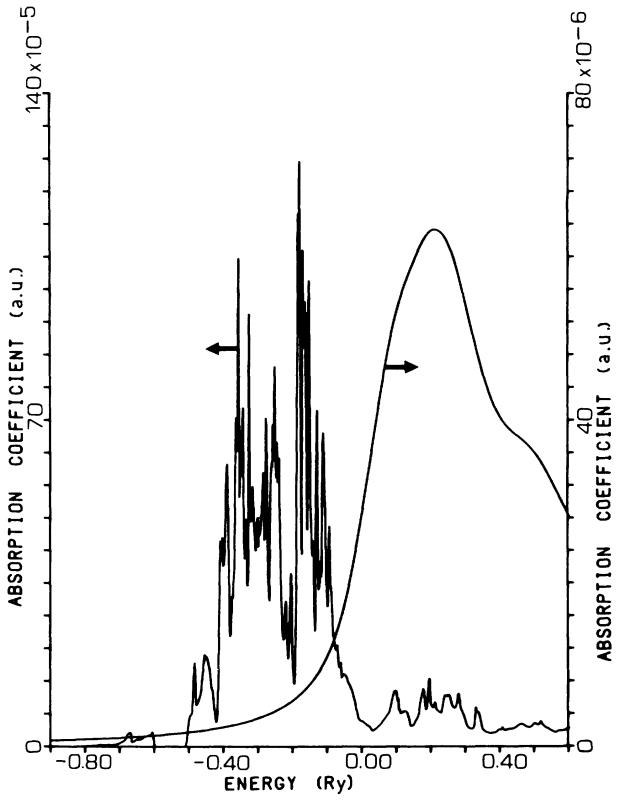

FIG. 11. Total raw spectrum (left axis) and absorption coefficient spectrum (right axis) of the Pd L_3 edge in Pd_2Si. The absorption coefficient has been computed taking into account the broadening due to the $2p_{3/2}$ core-hole lifetime, Eq. (4). The Fermi level is located at zero energy.

VI. TOTAL ENERGY AND RELATED QUANTITIES

The ground-state total energy of Pd_2Si has been evaluated through the density-functional formalism in LDA. The local-density theory provides a justification for the use of a one-electron potential in the calculation of ground-state properties, such as the total energy, and a prescription for constructing it.

The calculation has been performed at the experimental lattice parameters of Table I. In our frozen-core approach total energy differences equal the valence energy differences, due to the cancellation of some core orbital contributions.

The difference between the total energy of two Pd atoms plus one Si atom and the total energy of a Pd_2Si molecular unit in crystalline state gives the Pd_2Si cohesive energy. This computed value is shown in Table IV in units of Ry per atom, together with the values for elemental Pd (Ref. 11) and Si.[25] Their positive value represents stability of the solid relative to the free atom. Experimental cohesive energy, available only for Pd and Si,[26] are in good agreement with the computed values.

Since the only experimental information available about the energetics of Pd_2Si is the heat of formation, we calculated it by subtracting the Pd_2Si molecular unit (computed) cohesive energy from the (computed) cohesive energy of Si plus two times the (computed) cohesive energy of Pd. We note that all the three cohesive energies have been obtained with linear band-structure methods and with the same approximation to the exchange and correlation potential. The negative value of the computed heats of formation show that silicide is stable relative to segregated Si and Pd regions. As far as the comparison between theoretical and experimental value is concerned it should be considered that our estimate refers to the zero-temperature limit, while the measured data have been taken at room temperature. Furthermore, it should be remembered that calculation of the heat of formation is numerically very critical, because it is obtained from data (total energies) which are much greater than the resulting difference. For these reasons we consider our result very satisfactory and supporting the validity and accuracy of this calculation.

VII. DISCUSSION AND COMPARISON WITH THE EXPERIMENTS

A great deal of experimental work has been performed on transition-metal silicides in particular on Pd_2Si. We

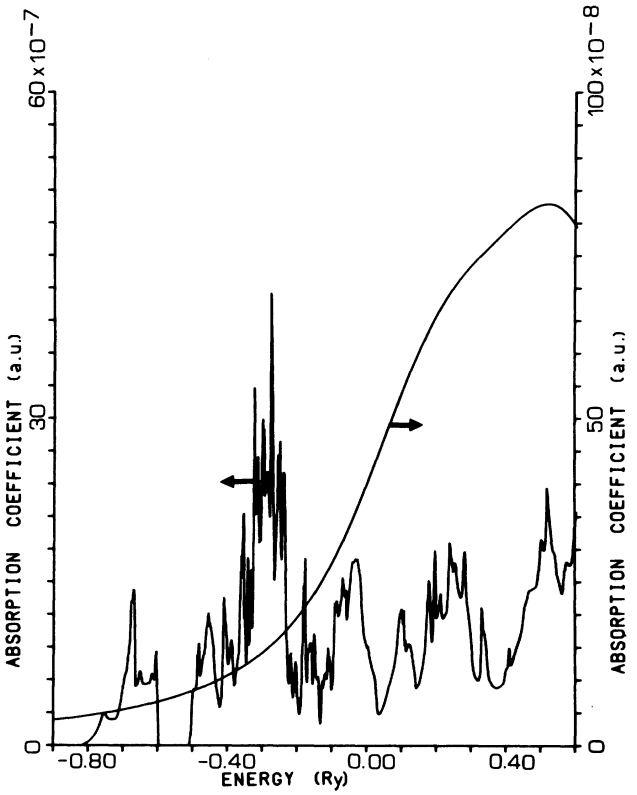

FIG. 12. Total raw spectrum (left axis) and absorption coefficient spectrum (right axis) of the Pd K edge in Pd_2Si. The absorption coefficient has been computed taking into account the broadening due to the 1s core-hole lifetime, Eq. (4). The Fermi level is located at zero energy.

will concentrate on the most recent one, which offers the greater amount of accurate information.

Part of the experiments have employed ultraviolet[27] or x-ray[28] radiation photoelectron spectroscopy to elucidate the band structure below the Fermi level. These spectra, owing to markedly different photoionization cross sections, are usually dominated by the d bands leaving the s-p states buried. The latter are revealed only by making use of the Cooper minimum or resonant photoemission technique.[29] Information on the Si s-p electronic states have been obtained by Auger electron spectroscopy[27,30] and by soft-x-ray emission spectroscopy,[31] while the Pd_2Si empty states have been investigated through x-ray absorption spectra[32,33] and bremsstrahlung isochromat spectroscopy (BIS).[34,35]

The data obtained from all these experiments are consistent with a simple picture of the electronic properties of palladium silicides. According to this model, first proposed by Riley *et al.*[36] for amorphous Pd-Si alloy, the compound formation leads to a narrowing of the main peak of the elemental Pd d band and shifts its center of gravity to higher binding energy. In addition the features characteristic of the Si—Pd bond appear as new d structures straddling the main d band. This bond can be described in terms of a bonding-antibonding Si p–Pd d interaction. The Si s electrons are not involved in the bond, and the consequent configuration of the Si atom is near the atomic one. This qualitative picture, which is confirmed by our study, has been successfully extended to other transition-metal silicides.[5]

Figure 13 shows some typical photoemission and BIS data of Pd_2Si compared with the computed total DOS of Fig. 4 after a 0.3 eV Gaussian broadening to simulate

TABLE IV. Computed total energies for valence electrons of atomic Pd and Si and for crystalline Pd_2Si. The cohesive energy is the difference between the total energy of the valence electrons in the crystal and in the atomic state. The difference between the cohesive energy of Si and Pd in crystalline elemental state and the cohesive energy in crystalline Pd_2Si state gives the zero-temperature heat of formation. Units are Ry/atom, i.e., the Pd_2Si cell values have been divided by the number of atoms in the cell (9).

	Pd	Si	Pd_2Si
Computed total valence energy	−60.2784 (atom)	−7.7876 (atom)	−43.1132 (crystal)
Computed cohesive energy	0.271[a]	0.3528[b]	0.3341
Experimental cohesive energy	0.2859[c]	0.3403[c]	?
Computed heat of formation (0 K)			−0.0358
Experimental heat of formation (300 K)			−0.0220[d]

[a] Reference 11.
[b] Reference 25.
[c] Reference 26.
[d] Reference 1.

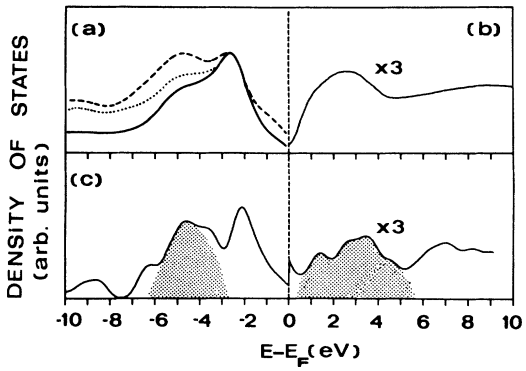

FIG. 13. Comparison between the experimental spectroscopic data for both occupied and unoccupied states and our computed Pd_2Si DOS. Curve (a) refers to the synchrotron radiation study of Ref. 29 at $h\nu=80$ eV (solid line), $h\nu=110$ eV (dashed line), and $h\nu=130$ eV (dotted line–Cooper minimum). Curve (b) shows the Bremsstrahlung isochromat spectroscopic result of Ref. 35. Curve (c) displays the total DOS curve of Fig. 4 after a 0.3 eV Gaussian broadening to simulate the experimental resolution. Dotted areas refers to Si p–Pd d states. The empty-states data have been expanded by a factor of 3.

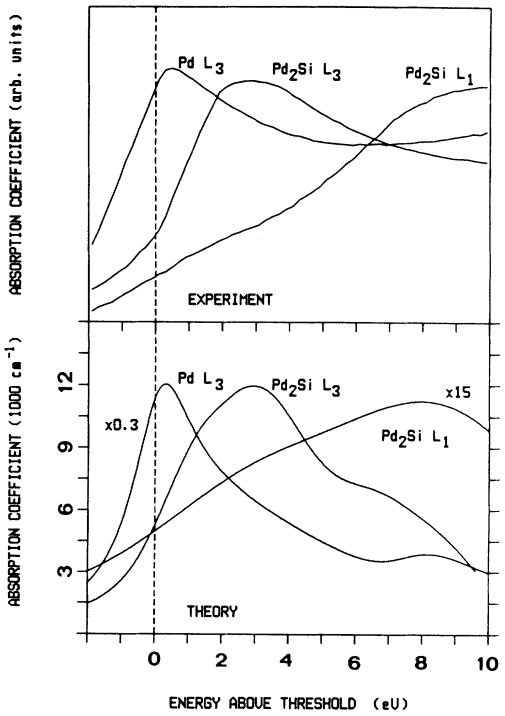

FIG. 14. Comparison between the experimental (upper panel) and theoretical (lower panel) L_1,L_3 x-ray absorption edges of Pd_2Si. XAS L_3 edge of pure Pd is also shown. Experimental data are from Ref. 33.

the experimental resolution.

Photoemission data have been measured with synchrotron radiation which allows us to exploit the energy dependence of the photoionization cross section to separate the contribution of the Si and Pd orbitals (Cooper minimum technique).[37–39] The partial photoionization cross section of 4d and 5d atomic orbitals, which is usually dominant, in Cooper minimum conditions shows a pronounced minimum, allowing us to investigate the Si contribution which would normally not be seen.[40] Therefore the spectrum in Fig. 13 at $h\nu=80$ eV probes the d orbitals, while at $h\nu=130$ eV (Cooper minimum) the Si sp states are detected. It is evident that all the information that such an analysis provide, i.e., energy location and shape of the main d band, of the Si s states and of the Si p–Pd d bonding features are in excellent agreement with our theoretical results. The presence of p states just below the Fermi level is also evident. The origin of this structure and the possibility that it might be attributed to the filled antibonding states have been discussed by various authors.[29,31,41,42]

The calculation in Ref. 18 showed that the Si p–Pd d antibonding states are unoccupied in Pd_3Si but partially filled in PdSi. It was, however, not clear what could be expected for Pd_2Si which has a stoichiometry intermediate between Pd_3Si and PdSi and with a complex structure different from the Cu_3Au and CuAu model geometries assumed in Ref. 18. The semiempirical calculation of Bisi and Calandra[19] predicted the antibonding states to start just above E_F, but this result was not considered conclusive due to the approximations in the tight-binding approach. For these reasons Franciosi and Weaver[29] concluded that the nature of the states within 1.5 eV around E_F was not certain. According to these authors there might be either a substantial amount of metal s-p character near E_F or the partially occupied antibonding states are the origin of the states below E_F. Grunthaner *et al.*[41,42] performed x-ray photoemission experiments and interpreted the emission below the Fermi level in terms of antibonding states. A similar conclusion has been reached by the recent soft x-ray emission experiment in Ref. 31.

It is now possible to settle the dispute. Our analysis of the projected DOS of Figs. 5–8 shows that these states originate from a Si p–Pd p coupling while the antibonding states are located entirely above the Fermi level.

Photoemission experiments have been performed not only on crystalline Pd_2Si but also at the reacted Si(111)-Pd interface.[38,43,44] The experimental information which has been obtained from these surface experiments are very similar to the results of Fig. 13 showing that the electronic properties of this interface are Pd_2Si-like.

As far as the empty-state region is concerned the BIS technique has been applied in the energy range up to 10 eV above E_F. The spectrum, shown in Fig. 13, is dominated by two well-defined structures with a minimum around 5 eV. It agrees very well with the theoretical DOS showing that the BIS spectra may be interpreted in terms of the density of states. The origin of these structures is different: the first, below 5 eV, is due to the Si p–Pd d antibonding interaction, while the second is due to Si d–Pd p coupling.

X-ray absorption (XAS) spectra provide information on the electronic properties of empty states too, but in

this experiment a hole, which may strongly interact with the valence electrons, is created in a core state. Much smaller is the perturbation present in a BIS experiment which is limited to the addition of an electron to the empty bands in the solid. For these reasons, while it is reasonable to compare BIS spectra with single-particle electronic states, the role of many-body effects in determining the XAS features is much more debated.[45] The many-body electron gas response to the x-ray transition corresponds to the interaction between the created core hole and a localized screening cloud of electrons of s-like symmetry. This excitation of the electron gas enhances the density of s states above the threshold. According to Citrin *et al.*[46] the inclusion of many-body effects has been found necessary for understanding the near edge spectra of simple metals, which are characterized by a free-electron behavior. In transition metals the situation is different since the s electrons play a secondary role compared to the d electrons. This leads to a simpler interpretation of the XAS spectra in terms of single-particle picture.[20–22,47]

Recently the response properties of Pd_2Si, which may be considered intermediate between those of a free-electron metal and those of a d-band metal, have been discussed. The measured pronounced resonance (white line) near the $L_{2,3}$ absorption threshold, has been interpreted in terms of either empty antibonding states[32] or many-body effects.[33] This last conclusion relies on an assumed small number of empty d states in Pd_2Si. Our calculations which are compared in Fig. 14 with the experimental data of Ref. 33 show that the one-electron picture may explain the photoabsorption spectra without any inclusion of many-body effects. In this figure we included also the elemental Pd L_3 edge, because it is interesting to compare the origin of the Pd and Pd_2Si L_3 while lines. The nature of the empty states involved in this transition is indeed different. In Pd these empty states are the tail of the main d band while in Pd_2Si they are the antibonding d states well above E_F. This difference leads to a separation of 2.4 eV between the two computed white line peaks. In order to refer the experimental spectra to the absorption threshold we fixed the binding energy of the core hole on the basis of x-ray photoemission measurements.[48,49] In this way we obtain an experimental separation between the Pd and Pd_2Si L_3 white lines of 2.3 eV in excellent agreement with our estimation. As far as the intensities are concerned we found a $I(Pd_2Si)/I(Pd)$ white line intensity ratio of 0.3. By considering that the Pd atoms in Pd_2Si are less dense by a factor of about 0.7, with respect, elemental Pd, the ratio, normalized to a single Pd atom, became 0.43. This result shows that the presence of empty d states and the enhancement effect due to the dipole matrix elements result in a strong structure in the L_3 spectra of Pd_2Si.

In Fig. 14 the L_1 is also shown. Again the computed single-particle photoabsorption spectrum is in good agreement with the experimental data. The main peak, due to the Pd $5p$ states is found at 7.9 eV in the calculation and at 9.8 eV in the measurement. The Si p–Pd d antibonding coupling produces a weak shoulder at 2.2 eV, to be compared with the corresponding experimental shoulder at 2.0 eV.

In conclusion we may note that all the experimental L_3 and L_1 Pd_2Si XAS structures can be interpreted in terms of the DOS calculated from the ground-state potential. The main peaks of these two spectra correspond to Pd $4d$ (L_3) and Pd $5p$ (L_1) states; the same states lead to the two structures seen by the BIS measurements. These results do not appear to be limited to Pd_2Si. According to del Pennino *et al.*,[50] the Ni $L_{2,3}$ absorption edges experiments in Ni_2Si may be interpreted in a similar way. Part of our empty-states results have been published earlier.[51]

Finally, our picture of the electronic states of Pd_2Si agrees with the Pettifor and Podloucky[52] theory of structural stability of p-d bonded compounds. These authors show that band energy plays a fundamental role in crystal stability. In other words, the structural energy is intimately related to the features in the density of states, its minimum value in NaCl and NiAs being due to a minimum in the density of states at E_F when all the p-d bonded orbitals are occupied. We found that in Pd_2Si the Fermi level lies in a minimum of the DOS, with all the p-d bonding states occupied and the antibonding empty. Furthermore, the role of s electrons is negligible as assumed in Ref. 52 and as explained by Gelatt *et al.*[53]

VIII. CONCLUSIONS

The main conclusion of this study may be summarized as follows. The basic bonding interaction between Pd and Si is due to a two-level coupling between Pd $4d$ and Si $3p$ orbitals, forming bonding-antibonding states straddling the main d structure. The bonding states are filled, the antibonding entirely unoccupied. The Si $3s$ states are found in a quasicore configuration.

The computed DOS shows well-defined features which cannot be interpreted in terms of the simple bonding-antibonding picture, but depend on the various and complex interactions which take place in the real Pd_2Si structure. Among them the Si $3p$–Pd $5p$ coupling responsible for the presence of Si p states just below E_F formerly attributed to antibonding states and the Si $3d$–Pd $5p$ which dominate the DOS spectrum around 8 eV above E_F.

The computed DOS are in excellent agreement with the results of different filled states spectroscopic experiments, like photoemission spectroscopy and x-ray emission spectroscopy. The empty states have been investigated both by comparing the ground-state DOS with the BIS spectra and by computing the x-ray photoabsorption spectra. The two well-defined peaks in the BIS curve are due to the presence of the Si p–Pd d antibonding states and to the Si d–Pd p structure. Furthermore, we found that a single-particle picture can interpret the x-ray absorption spectra and explain the occurrence of a white line at the $L_{2,3}$ edge. We found that the same two structures detected by BIS are responsible for the dominant

features in the x-ray absorption spectra, one in the $L_{2,3}$ edge, the other in the K and L_1 edge. The computed cohesive energy and heat of formation agrees with the stability of this compound and with the available experimental data.

ACKNOWLEDGMENTS

One of us (O.B.) thanks the Max-Planck-Institut for its hospitality. Financial support by Consiglio Nazionale delle Ricerche is acknowledged.

[1]K. N. Tu and J. W. Mayer, in *Thin Films-Interdiffusion and Interactions,* edited by J. M. Poate, K. N. Tu, and J. W. Mayer (Wiley, New York, 1978), p. 359.

[2]S. P. Murarka, *Silicides for VLSI Applications* (Academic, New York, 1983).

[3]G. W. Rubloff, in *Festkörperprobleme (Advances in Solid State Physics),* edited by P. Grose (Vieweg, Braunschweig, 1983), Vol. 23, p. 179.

[4]P. S. Ho, J. Vac. Sci. Technol. A **1**, 745 (1983).

[5]C. Calandra, O. Bisi, and G. Ottaviani, Surf. Sci. Rep. **4**, 271 (1985).

[6]L. Hedin and B. I. Lundqvist, J. Phys. C **4**, 2064 (1971).

[7]P. Hohenberg and W. Kohn, Phys. Rev. **136**, B864 (1964).

[8]W. Kohn and L. J. Sham, Phys. Rev. **140**, A1133 (1965).

[9]A. R. Mackintosh and O. K. Andersen, in *Electrons at the Fermi Surface,* edited by M. Springford (Cambridge University Press, Cambridge, 1980).

[10]V. L. Moruzzi, J. F. Janak, and A. R. Williams, *Calculated Electronic Properties of Metals* (Pergamon, New York, 1978).

[11]O. K. Andersen, Phys. Rev. B **12**, 3060 (1975).

[12]W. B. Pearson, *Handbook of Lattice Spacing and Structures of Metals and Alloys* (Pergamon, New York, 1958).

[13]W. D. Buckey and S. C. Moss. Solid State Electron. **15**, 1331 (1972).

[14]O. K. Andersen, in *The Electronic Structure of Complex Systems,* edited by P. Phariseau and W. M. Temmerman (Plenum, New York, 1984).

[15]H. L. Skriver, *The LMTO Method* (Springer, Berlin, 1984).

[16]E. Clementi and C. Roetti, At. Data Nucl. Data Tables **14**, 177 (1974).

[17]O. Jepsen and O. K. Andersen, Solid State Commun. **9**, 1763 (1971).

[18]P. S. Ho, G. W. Rubloff, J. E. Lewis, V. L. Moruzzi, and A. R. Williams, Phys. Rev. B **22**, 4784 (1980).

[19]O. Bisi and C. Calandra, J. Phys. C **14**, 5479 (1981).

[20]J. E. Muller, O. Jepsen, O. K. Andersen, and J. W. Wilkins, Phys. Rev. Lett. **40**, 720 (1978).

[21]J. E. Muller, O. Jepsen, and J. W. Wilkins, Solid State Commun. **42**, 365 (1982).

[22]J. E. Muller and J. W. Wilkins, Phys. Rev. B **29**, 4331 (1984).

[23]K. D. Sevier, *Low-Energy Electron Spectrometry* (Wiley-Interscience, New York, 1972), Chap. 6.

[24]O. Keski-Rahkonen and M. O. Krause, At. Data Nucl. Data Tables **14**, 139 (1974).

[25]D. Glötzel, B. Segall, and O. K. Andersen, Solid State Commun. **36**, 403 (1980).

[26]C. Kittel, *Introduction to Solid State Physics,* 4th ed. (Wiley, New York, 1971).

[27]P. S. Ho, G. W. Rubloff, J. E. Lewis, V. L. Moruzzi, and A. R. Williams, Phys. Rev. B **22**, 4784 (1980).

[28]P. J. Grunthaner, F. J. Grunthaner, A. Madhukar, and J. W. Mayer, J. Vac. Sci. Technol. **19**, 649 (1981).

[29]A. Franciosi and J. H. Weaver, Phys. Rev. B **27**, 3554 (1983).

[30]O. Bisi, in *Thin-Films-Interfaces and Phenomena,* edited by R. J. Nemanich, P. S. Ho, and S. S. Lau (Materials Research Society, Pittsburgh, 1986), p. 13.

[31]K. Tanaka, T. Saito, K. Suzuki, and R. Hasagawa, Phys. Rev. B **32**, 6853 (1985).

[32]G. Rossi, R. Jaeger, J. Stohr, T. Kendelewicz, and I. Lindau, Phys. Rev. B **27**, 5154 (1983).

[33]M. De Crescenzi, E. Colavita, U. del Pennino, P. Sassaroli, S. Valeri, C. Rinaldi, L. Sorba, and S. Nannarone, Phys. Rev. B **32**, 612 (1985).

[34]F. J. Himpsel and Th. Fauster, J. Vac. Sci. Technol. A **2**, 815 (1984).

[35]D. D. Sarma, F. U. Hillebrecht, M. Campagna, C. Carbone, J. Nogami, I. Lindau, T. W. Barbee, L. Braicovich, I. Abbati, and B. De Michelis, Z. Phys. B **59**, 159 (1985).

[36]J. D. Riley, L. Ley, J. Azoulay, and K. Terakura, Phys. Rev. B **20**, 776 (1979).

[37]J. W. Cooper, Phys. Rev. **128**, 681 (1962).

[38]J. N. Miller, S. A. Schwarz, I. Lindau, W. E. Spicer, B. De Michelis, I. Abbati, and L. Braicovich, J. Vac. Sci. Technol. **17**, 920 (1980).

[39]I. Abbati, G. Rossi, L. Braicovich, I. Lindau, and W. E. Spicer, J. Vac. Sci. Technol. **19**, 636 (1981).

[40]G. Rossi, I. Lindau, L. Braicovich, and I. Abbati, Phys. Rev. B **28**, 3031 (1983).

[41]P. J. Grunthaner, F. J. Grunthaner, and A. Madhukar, J. Vac. Sci. Technol. **20**, 680 (1982).

[42]P. J. Grunthaner, F. J. Grunthaner, and A. Madhukar, Physica **117B-118B**, 831 (1983).

[43]P. S. Ho, P. E. Schmid, and H. Foll, Phys. Rev. Lett. **46**, 782 (1981).

[44]L. Braicovich, Surf. Sci. **132**, 315 (1983).

[45]G. D. Mahan, in *Solid State Physics,* edited by H. Ehrenreich, F. Seitz, and D. Turnbull (Academic, New York, 1974), Vol. 29, p. 75.

[46]P. H. Citrin, G. K. Wertheim, and M. Schluter, Phys. Rev. B **20**, 3067 (1979).

[47]T. K. Sham, Phys. Rev. B **31**, 1888 (1985).

[48]J. A. Bearden and A. F. Burr, Rev. Mod. Phys. **39**, 125 (1967).

[49]The Pd_2Si core levels binding energy has been evaluated by shifting the corresponding Pd level by 1.4 eV, which is the difference between the Pd and Pd_2Si $3d_{5/2}$ core-level energy location as determined in Ref. 37.

[50]U. del Pennino, C. Mariani, S. Valeri, G. Ottaviani, M. G. Betti, S. Nannarone, and M. De Crescenzi, Phys. Rev. B **34**, 2875 (1986).

[51]O. Bisi, O. Jepsen, and O. K. Andersen, Europhys. Lett. **1**, 149 (1986).

[52]D. G. Pettifor and R. Podloucky, Phys. Rev. Lett. **53**, 1080 (1984).

[53]C. D. Gelatt, Jr., A. R. Williams, and V. L. Moruzzi, Phys. Rev. B **27**, 2005 (1983).